Excitation energies from real-time propagation of the four-component Dirac–Kohn–Sham equation

Michal Repisky,[*,†] Lukas Konecny,[‡] Marius Kadek,[†] Stanislav Komorovsky,[†] Olga L. Malkina,[¶,‡] Vladimir G. Malkin,[¶] and Kenneth Ruud[†]

The Centre for Theoretical and Computational Chemistry, Department of Chemistry, UiT The Arctic University of Norway, Tromsø, Norway, Department of Inorganic Chemistry, Faculty of Natural Sciences, Comenius University, Bratislava, Slovak Republic, and Institute of Inorganic Chemistry, Slovak Academy of Sciences, Bratislava, Slovak Republic

E-mail: michal.repisky@uit.no

Abstract

We report the first implementation of real-time time-dependent density functional theory (RT-TDDFT) at the relativistic four-component level of theory. In contrast to the perturbative linear-response TDDFT approach (LR-TDDFT), the RT-TDDFT approach performs an explicit time propagation of the Dirac–Kohn–Sham density matrix, offering the possibility to simulate molecular spectroscopies involving strong electromagnetic fields while at the same time treating relativistic scalar and spin–orbit corrections variationally. The implementation is based on the matrix representation of the

---

[*]To whom correspondence should be addressed
[†]The Centre for Theoretical and Computational Chemistry, Department of Chemistry, UiT The Arctic University of Norway, Tromsø, Norway
[‡]Department of Inorganic Chemistry, Faculty of Natural Sciences, Comenius University, Bratislava, Slovak Republic
[¶]Institute of Inorganic Chemistry, Slovak Academy of Sciences, Bratislava, Slovak Republic

Dirac–Coulomb Hamiltonian in the basis of restricted kinetically balanced Gaussian-type functions, exploiting the non-collinear Kramers unrestricted formalism implemented in the program ReSpect. We also present an analytic form for the delta-type impulse commonly used in RT-TDDFT calculations as well as a dipole-weighted transition matrix analysis facilitating the interpretation of spectral transitions in terms of ground-state molecular orbitals. The possibilities offered by the methodology are illustrated by investigating vertical excitation energies and oscillator strengths for ground-to excited-state transitions in the group 12 atoms and in heavy-element hydrides. The accuracy of the method is assessed by comparing the excitation energies obtained with earlier relativistic linear response TDDFT results and available experimental data.

1   Introduction

The response of molecular systems to external fields forms the basis for a vast number of molecular spectroscopic parameters that can be accurately modelled in the weak-field limit using the tools of quantum chemistry.[1] In this limit the applied fields typically induce only a small perturbation of the molecular ground state, and thus approaches based on response theory provide an adequate theoretical foundation for calculating many spectroscopic parameters.[1] An interesting example is linear response time-dependent density functional theory (LR-TDDFT) which has become the most prominent quantum chemistry method for the calculation of electronic excitation energies of atoms and molecules.[2–5]

In general, however, approaches based on response theory are insufficient to study molecular systems in strong fields. For instance, recent advances in experimental ultrafast spectroscopy have made it possible to obtain spectral information about numerous chemical processes at the femto- and atto-second time scale, usign high-intensity laser pulses with wavelengths ranging from the far infrared to the far ultraviolet region.[6] In this case, the fundamental physics of light–matter interactions has revealed fast non-equilibrium dynamics of electrons (and nuclei), and accurate theoretical modeling of such processes requires

non-linear time-resolved methods. Among explicit time-propagation approaches, real-time time-dependent density functional theory (RT-TDDFT) has gained popularity due to its favorable trade-off between computational cost and accuracy, which has stimulated an interest in ultrafast structural dynamic simulations.[7–27] The only added computational and implementational effort associated with the real-time TDDFT approach is the development of an accurate and stable time propagator and the explicit formation of the Fock matrix at each time step. This complication is however compensated by several advantageous features of RT-TDDFT method such as a reduced asymptotic scaling behavior of the algorithm, the absence of explicit exchange-correlation kernel derivatives,[28] the absence of divergence problems appearing in response theory at resonant frequencies, and the implementational simplicity, involving essentially only routines for ground-state density optimization.

In recent years, several non-relativistic implementations of real-time TDDFT have been reported in literature. Most of the implementations follow the pioneering works of Theilhaber,[7] and Yabana and Bertsch,[8] and utilize a real-space grid methodology.[9] Among alternative techniques, the numerical basis sets accompanied with pseudopotentials for core-electrons,[10] as well as analytic atom-centered Gaussian basis functions[11–14] have gained popularity in recent years. The real-time TDDFT approach has been used in numerous applications to study, for instance, linear[14–17] and non-linear optical response properties,[18–21] molecular conductance,[22] singlet–triplet transitions,[23] magnetic circular dichroism,[24] core excitations,[13,25] photoinduced electric currents,[26] and plasmon resonances.[27]

For systems containing heavy elements, however, reliable theoretical models should account for relativistic corrections, of which the most important contribution for excitation energies is the spin–orbit coupling. Therefore, a rigorous starting point for the development of relativistic TDDFT is the four-component formalism based on the Dirac Hamiltonian. Such a development has recently been materialized in the linear-response TDDFT (LR-TDDFT) implementation by Gao and coworkers.[29] The original approach has later been improved by using a non-collinear form for the exchange–correlation kernel,[30] and extended further by

3

Bast *et al.*[31] to hybrid GGA functionals with a rigorous analytic expression for the exchange–correlation kernels. In the present work, however, we have examined an alternative route to model electronic excitation processes in molecular systems containing heavy elements, such that the four-component Dirac–Kohn–Sham equation will be solved directly in the real-time domain. We employ the matrix representation of the Dirac–Coulomb Hamiltonian using a time-independent basis of restricted kinetically balanced Gaussian-type functions. This is the first implementation and application of the four-component RT-TDDFT to atomic and molecular systems. The present relativistic RT-TDDFT formalism offers, in contrast to the linear-response TDDFT approach, also the possibility to simulate a wide range of spectroscopic techniques involving strong electromagnetic fields, variationally including the electron-spin degrees of freedom as well as relativistic scalar and spin–orbit corrections. The importance of the present formalism has been examined for hydrogenlike systems by Selstø *et al.*,[32] and in the perspective of relativistic quantum chemistry recently reviewed by Belpassi *et al.*.[33] The present methodology is particularly desirable because it represents an important step forward towards the understanding of relativistic and spin-dynamic effects in optical properties, high-harmonic generation, and molecular electronic transport properties.

The remainder of the article is organized as follows: In Section 2.1, we review basic RT-TDSCF methodology, both at Hartree–Fock (RT-TDHF) and density functional level of theory (RT-TDDFT), focusing on the structure of the four-component time-dependent Fock matrix. Computational details are given in Section 3 and the possibilities offered by the methodology are illustrated in Section 4 by calculations of excited-state transitions for the group 12 atoms and heavy-element hydrides. Concluding remarks and perspectives are drawn in Section 5.

2   Theory

In this section, we present the theoretical foundation for our implementation of the four-component relativistic RT-TDSCF methodology based on Hartree–Fock (RT-TDHF) and density functional theory (RT-TDDFT). Unless otherwise specified, atomic units are used throughout the paper. We first discuss the basic equations for the RT-TDSCF theory in Section 2.1, before we discuss in more detail the approach for integrating the RT-TDSCF equation in Section 2.2. Section 2.3 discusses how electron absorption spectra can be obtained from the RT-TDSCF calculations. In Section 2.4, we present a way to introduce an analytic, instead of numerical, expression for δ-function type perturbations, before we finally in Section 2.5 present a scheme for analysing the excited-state transitions.

2.1   Real-time time-dependent self-consistent field (RT-TDSCF) method

The starting point for RT-TDSCF methods such as Hartree-Fock (RT-TDHF) and density functional theory (RT-TDDFT) is the Liouville–von Neumann equation. In an orthonormal basis, the Liouville–von Neumann equation has in the formulation using the one-electron reduced density matrix the form[34]

$$i\frac{\partial \mathbf{D}^{\mathrm{MO}}(t)}{\partial t} = \left[\mathbf{F}^{\mathrm{MO}}(t), \mathbf{D}^{\mathrm{MO}}(t)\right], \tag{1}$$

where t is the time variable, i is the imaginary unit, and $[\mathbf{A}, \mathbf{B}] = \mathbf{A}\mathbf{B} - \mathbf{B}\mathbf{A}$ denotes the commutator between two matrices $\mathbf{A}$ and $\mathbf{B}$. In Eq. (1), $\mathbf{F}^{\mathrm{MO}}(t)$ is the time-dependent Fock matrix and $\mathbf{D}^{\mathrm{MO}}(t)$ the one-particle reduced density matrix. The Fock and density matrices are expressed in an orthonormal basis and can be either non-relativistic or relativistic. In our implementation, we use the reference molecular orbitals (MO) obtained from the solution of the static (time-independent) self-consistent field (SCF) equation. In contrast to LR-

TDDFT for excited states,[2–5] we solve Eq. (1) explicitly in the time domain by propagating the density matrix in time.

At the initial time $t_0 = 0$, both the optimized Fock and density matrices have a well-defined diagonal form

$$\mathbf{D}_0^{\mathrm{MO}} \equiv \mathbf{D}^{\mathrm{MO}}(t{=}0) = \begin{pmatrix} \mathbf{1}_{\mathrm{oo}} & \mathbf{0}_{\mathrm{ov}} \\ \mathbf{0}_{\mathrm{vo}} & \mathbf{0}_{\mathrm{vv}} \end{pmatrix} ; \qquad \mathbf{F}_0^{\mathrm{MO}} \equiv \mathbf{F}^{\mathrm{MO}}(t{=}0) = \begin{pmatrix} \varepsilon_1 & \cdots & 0 \\ \vdots & \ddots & \vdots \\ 0 & \cdots & \varepsilon_n \end{pmatrix}, \qquad (2)$$

where for a single-particle basis of size n, $\{\varepsilon\}$ is the set of n unperturbed molecular orbital energies, and $\mathbf{1}_{\mathrm{oo}}$ is the identity matrix of dimension $N \times N$ associated with the occupied (o) one-particle states of an N-electron system. The remaining blocks of $\mathbf{D}_0^{\mathrm{MO}}$ consist of zero matrices, where the dimension v refers to the number of virtual orbitals. In the case of relativistic four-component theory, the reference to the virtual space also includes all negative-energy eigenstates of the Dirac–Fock operator.

Within a finite time window, the solution of the Liouville–von Neumann equation Eq. (1) reduces to the evaluation of the time-dependent Fock matrix at discrete time-steps, and to propagating the density matrix in time. A detailed discussion on the density matrix propagation is left for Section 2.2. Here, we only briefly outline the main features of the Fock matrix calculation, which is initially evaluated in the basis of the static (time-independent) atomic orbitals (AO) by means of an integral-direct algorithm and subsequently transfered to the reference MO basis. At each time t, the Fock matrix remains Hermitian and can be written in the formalism suitable for Hartree–Fock and Kohn–Sham theory as

$$\mathbf{F}^{\mathrm{AO}}(t) = \mathbf{h} + \mathbf{G}[\alpha, \mathbf{D}^{\mathrm{AO}}(t)] + \mathbf{V}^{\mathrm{XC}}[(1 - \alpha), \rho(t)] + \mathbf{V}^{\mathrm{ext}}(t). \qquad (3)$$

Here, $\mathbf{h}$ is the matrix representation of the time-independent one-electron Hamiltonian, and $\mathbf{G}$ is the two-electron interaction matrix. The scalar coefficient α weights the admixture

of the Hartree–Fock exchange contribution with the DFT exchange-correlation potential matrix $\mathbf{V}^{\mathrm{XC}}$, giving rise to pure TDHF ($\alpha = 1$), pure TDDFT ($\alpha = 0$), or hybrid schemes ($0 < \alpha < 1$). The time-dependent external potential $\mathbf{V}^{\mathrm{ext}}(t)$ accounts for the interaction of the molecular system with an applied external electric field. Within a dipolar coupling approximation, the wavelength of the incoming photons is assumed to be much larger than the system size, and then the perturbation potential has a simple form of the electric dipole operator, details of which will be discussed in Section 2.3. To solve Eq. (1), the Fock matrix is transformed from an AO basis to the reference MO basis at each time-step using the reference MO expansion coefficients $\mathbf{C}$

$$\mathbf{F}^{\mathrm{MO}}(t) = \mathbf{C}^{\dagger}\mathbf{F}^{\mathrm{AO}}(t)\mathbf{C}. \tag{4}$$

The same coefficients are also used for the evaluation of AO density matrix in Eq. (3)

$$\mathbf{D}^{\mathrm{AO}}(t) = \mathbf{C}\mathbf{D}^{\mathrm{MO}}(t)\mathbf{C}^{\dagger}. \tag{5}$$

A novel feature of the present RT-TDSCF implementation is the use of full four-component relativistic formalism based on the Dirac–Coulomb Hamiltonian for the calculation of excitation energies. The approach takes into account both scalar and spin-same-orbit interactions variationally, probing finer details in the absorption spectra caused by relativistic effects. This formalism extends the applicability of RT-TDSCF to molecular systems with significant relativistic effects. All those benefits comes, however, at the expense of higher computational cost and complexity, primarily due to the need for evaluating integrals over two distinct sets of basis functions, $\{\chi\} = \{\chi^{\mathrm{L}}, \chi^{\mathrm{S}}\}$. Each of the so-called large $\{\chi^{\mathrm{L}}\}$ and small component $\{\chi^{\mathrm{S}}\}$ basis sets consists of two-component spinors, governed to lowest order in c^{-2} (c being the speed of light) by the restricted kinetically balanced relation (RKB):[35] $\{\chi^{\mathrm{S}}\} = \{(\boldsymbol{\sigma}\cdot\mathbf{p})\chi^{\mathrm{L}}\}$, where $\boldsymbol{\sigma}$ is the vector of three Pauli spin matrices. Obvious complications arise from the presence of momentum operator, $\mathbf{p} = -i\boldsymbol{\nabla}$ in the expression for the small-

component basis functions. In particular, the evaluation of electron repulsion integrals (ERI) over the basis functions is the source of most difficulties in the four-component electronic structure theory, especially when compared with methods based on one- or two-component Hamiltonians. We will here take advantage of our recent developments methods suited for the efficient evaluation of relativistic two-electron integrals.[36]

We will in the following assume that all terms in Eq. (3) arise from the relativistic four-component theory based on the Dirac–Coulomb Hamiltonian. For simplicity, these contributions will be presented in a more compact two-by-two representation where L and S superscripts denote the large- and small-component, respectively. $\mathbf{h}$ is then the matrix representation of the time-independent one-electron Dirac Hamiltonian in the field of clamped nuclei

$$\mathbf{h} = \begin{bmatrix} \mathbf{V}^{\text{Ne}} & c\mathbf{T} \\ c\mathbf{T} & \mathbf{W}^{\text{Ne}} - 2c^2\mathbf{T} \end{bmatrix},$$ (6)

where $\mathbf{T}$ is the kinetic energy matrix, c is the speed of light, and $\mathbf{V}^{\text{Ne}}$ ($\mathbf{W}^{\text{Ne}}$) is the nuclear–electron attraction matrix over the large- (small-)component basis.[37] In contrast to the one-electron part, there is no closed relativistic expression for the two-electron interaction. Instead, a perturbation expansion in c^{-2} is used to identify the leading-order two-electron relativistic contribution, known as the frequency-independent Breit interaction. Even though, the Breit interaction may be included in the zeroth-order Hamiltonian variationally,[38] the fast evaluation of two-electron integrals over the resulting Coulomb–Breit Hamiltonian still represents a challenging task. It is also well known that the lost of accuracy associated with the use of approximate DFT functionals is larger than the effect of neglected the Breit interaction. It is therefore common in modern relativistic quantum chemistry to take into account only the leading-order Coulomb Hamiltonian, $1/r_{12}$, and to represent the electron-electron interaction matrix $\mathbf{G}$ by the instantaneous Coulomb interaction matrix $\mathbf{J}$ and the

8

Hartree–Fock exchange matrix $\mathbf{K}$,[39]

$$\mathbf{G}(\alpha) = \mathbf{J} - \alpha\mathbf{K} = \begin{bmatrix} \mathbf{J}^{\mathrm{LL}} & \mathbf{0}_{2\times 2} \\ \mathbf{0}_{2\times 2} & \mathbf{J}^{\mathrm{SS}} \end{bmatrix} - \alpha \begin{bmatrix} \mathbf{K}^{\mathrm{LL}} & \mathbf{K}^{\mathrm{LS}} \\ \mathbf{K}^{\mathrm{SL}} & \mathbf{K}^{\mathrm{SS}} \end{bmatrix}. \tag{7}$$

The remaining contribution in Eq. (3), $\mathbf{V}^{\mathrm{XC}}$, arises from DFT and accounts for the non-classical effects of exchange and correlation. In relativistic TDDFT, this term typically accommodates two approximations: The first is the adiabatic approximation, where the dependence of the exchange–correlation functional on the densities at all times in the past is approximated by the ground-state form of the functional, *i.e.*

$$\mathbf{V}^{\mathrm{XC}}[\rho, \boldsymbol{\nabla}\rho](\boldsymbol{r}, t) \approx \mathbf{V}^{\mathrm{XC}}[\rho_t, \boldsymbol{\nabla}\rho_t](\boldsymbol{r})\big|_{\rho_t = \rho(\boldsymbol{r}, t)}. \tag{8}$$

In this case, the time-dependence of functionals is only implicit via the electron density, $\rho(t)$, and gradients of the density. The second approximation is the use of a non-relativistic exchange–correlation functionals, as there are no exchange–correlation functionals explicitly designed for relativistic calculations.[40] Here, it is important to note that the rotational invariance of non-relativistic spin-density functionals is not automatically preserved in a relativistic formalism. To circumvent this problem, we take advantage of the non-collinear approach proposed by van Wüllen.[41]

2.2 Integration of the RT-TDSCF equation

The solution of the Liouville–von Neumann equation Eq. (1) can in its most general form be written as[42]

$$\mathbf{D}(t) = \mathbf{U}(t, t_0)\, \mathbf{D}(t_0)\, \mathbf{U}^{\dagger}(t, t_0), \tag{9}$$

where $\mathbf{U}(t, t_0)$ is the unitary evolution operator propagating the density matrix from time t_0 to time t. The evolution operator can be formally expressed as

$$\mathbf{U}(t, t_0) = \mathcal{T} \exp\left[-i \int_{t_0}^{t} \mathbf{F}(\tau) d\tau\right], \tag{10}$$

where the exponential form of the operator is defined by its Taylor series. The time ordering operator $\mathcal{T}$ indicates that all expansion terms in the exponent are time-ordered:[42]

$$\mathcal{T} \exp\left[-i \int_{t_0}^{t} \mathbf{F}(\tau) d\tau\right] = \sum_{n=0}^{\infty} \frac{(-i)^n}{n!} \int_{t_0}^{t} d\tau_1 \int_{t_0}^{t} d\tau_2 \ldots \int_{t_0}^{t} d\tau_n \times \mathcal{T}[\mathbf{F}(\tau_1)\mathbf{F}(\tau_2) \ldots \mathbf{F}(\tau_n)]. \tag{11}$$

The time ordering is necessary because the Fock operator depends on time, both explicitly and implicitly, and therefore does not commute with itself when expressed at different times. The time dependence of the Fock operator persists in the RT-TDSCF formalism even in the absence of an external time-dependent field, since the Fock operator depends on time through the molecular orbitals (see Eq. (3)). This fact puts demands on the propagation scheme: the time ordering has to be accounted for. There are two classes of propagators, global and local.[43] Global propagators such as the Taylor, Chebychev or Lanczos methods[43,44] are intended to propagate the system between two arbitrary times t_0 and t and as such can only be used for equations with time-independent operator (Hamiltonian). In the context of RT-TDSCF method (or more generally non-linear problems) the global propagators can only be used to propagate the system between two times that differ by a very small time step Δt.[44] The whole time interval is then expressed as a series of local propagations defined by this small time step. Alternatively, one can use specially designed local propagators such as the Crank-Nichloson method, Runge-Kutta or the Magnus method.[44] The latter has been chosen for our implementation and is discussed in the next paragraphs. For more details on methods for propagating the electron density in time, we refer to recent reviews.[43–45]

A good propagation method should preserve the time-reversal symmetry of the original equation of motion, as well as the unitarity of the evolution operator. The latter condition

is essential for preserving the time-reversal symmetry, trace and idempotency conditions of the density matrix. It is important to remark here that the time-reversal invariance would break in the presence of magnetic interactions. These demands are satisfied by the Magnus expansion[46] based propagator for numerically solving the TDSCF equation of motion (1). In this approach, the evolution operator (10) is written as an infinite series, thus avoiding the use of the time ordering operator

$$\mathbf{U}(t, t_0) = \exp\left[\mathbf{A}_1(t, t_0) + \mathbf{A}_2(t, t_0) + \ldots\right], \tag{12}$$

where the first three terms are defined as

$$\mathbf{A}_1(t, t_0) \equiv -i \int_{t_0}^t d\tau \mathbf{F}(\tau), \tag{13}$$

$$\mathbf{A}_2(t, t_0) \equiv -\frac{1}{2}(-i)^2 \int_{t_0}^t d\tau_2 \int_{t_0}^{\tau_2} d\tau_1 \left[\mathbf{F}(\tau_1), \mathbf{F}(\tau_2)\right], \tag{14}$$

$$\mathbf{A}_3(t, t_0) \equiv -\frac{1}{6}(-i)^3 \int_{t_0}^t d\tau_3 \int_{t_0}^{\tau_3} d\tau_2 \int_{t_0}^{\tau_2} d\tau_1 \left[\mathbf{F}(\tau_1), \left[\mathbf{F}(\tau_2), \mathbf{F}(\tau_3)\right]\right] + \left[\left[\mathbf{F}(\tau_1), \mathbf{F}(\tau_2)\right], \mathbf{F}(\tau_3)\right]. \tag{15}$$

For short time intervals, the evolution operator can be approximated by truncating the expansion (12)[44] and the integrals can be evaluated using numerical quadrature. For example, the mid-point rule for the first term in Eq. (13) gives

$$\mathbf{U}(t + \Delta t, t) \approx \exp\left[\mathbf{A}_1(t + \Delta t, t)\right] \approx \exp\left[-i\mathbf{F}\left(t + \frac{\Delta t}{2}\right) \cdot \Delta t\right]. \tag{16}$$

The mid-point rule is a second-order method (the error being proportional to Δt^3), and the approach is therefore often referred to as the second-order mid-point Magnus propagator.[14,44] By restricting instead the evolution operator to the first two terms of the Magnus expansion $\mathbf{U}(t + \Delta t, t) \approx \exp[\mathbf{A}_1(t + \Delta t, t) + \mathbf{A}_2(t + \Delta t, t)]$ we obtain the fourth-order Magnus method.[44] However, it has been shown that unless there is a strong time dependence in the Hamiltonian,

e.g. from a rapidly oscillating external field, the second-order Magnus method can be used to obtain accurate results.[44]

In the second-order mid-point Magnus propagator approach, the density matrix is updated using

$$\mathbf{D}^{\mathrm{MO}}(t + \Delta t) = \mathbf{U}(t + \Delta t, t)\, \mathbf{D}^{\mathrm{MO}}(t)\, \mathbf{U}^{\dagger}(t + \Delta t, t), \tag{17}$$

where the evolution operator is calculated using the Fock matrix [see Eq. (16)]. This requires the calculation of the Fock matrix at time $t + \Delta t/2$ where no density matrix is available. The mid-point Fock matrix can be obtained by an extrapolation from $\mathbf{F}(t)$, although this may have a negative effect on the accuracy of the calculations (the same problem arises in the beginning of the calculation when only the density matrix at time $t = 0$ is known). One possibility to improve the accuracy is to use a predictor–corrector algorithm (see for example Ref.[22]). To solve this issue, we employ an iterative series of extrapolations and interpolations in each time step.[25,44] In this method, as a first step, the mid-point Fock matrix is obtained by extrapolating the data from the previous time step

$$\mathbf{F}\left(t + \frac{\Delta t}{2}\right) = 2\mathbf{F}(t) - \mathbf{F}\left(t - \frac{\Delta t}{2}\right). \tag{18}$$

The density matrix $\mathbf{D}(t + \Delta t)$ and the corresponding Fock matrix $\mathbf{F}(t + \Delta t)$ are then calculated using Eq. (17). Finally the mid-point Fock matrix is constructed by interpolation

$$\mathbf{F}\left(t + \frac{\Delta t}{2}\right) = \frac{1}{2}\mathbf{F}(t) + \frac{1}{2}\mathbf{F}(t + \Delta t), \tag{19}$$

and thus closing the iteration cycle. The calculation of the $\mathbf{D}(t + \Delta t)$ and $\mathbf{F}(t + \Delta t)$ matrices and the interpolation step are repeated until convergence is reached. An example of the convergence criterion chosen in our implementation is the Euclidean norm of the difference between density matrices obtained in the n-th and $(n + 1)$-st iteration that has to be lower than some predefined threshold.

2.3 Electron absorption spectra from RT-TDSCF

To obtain excitation energies and absorption spectra from real-time simulations, the molecular system is perturbed by applying an external time-dependent electric field $\boldsymbol{\varepsilon}(\boldsymbol{r}, t)$. In our case, we study molecular systems that are small compared to wavelengths of the incoming light. Therefore, we can assume the dipole approximation in which the interaction potential in Eq. (3) takes the form

$$\mathbf{V}^{\text{ext}}(t) = - \sum_{\alpha=x,y,z} \mathbf{P}_\alpha \varepsilon_\alpha(t), \tag{20}$$

where $\mathbf{P}_\alpha$ is the matrix representation of the electric dipole moment operator, $-\mathbf{r}_\alpha$. The importance of contributions beyond the dipole approximation was recently investigated by Bernadotte *et al.*[47] and found to be small even for energies of the incoming photons being in relevant ranges for X-ray spectroscopy. Finally, an infinitely narrow impulse was chosen for $\varepsilon_\alpha(t)$ in Eq. (20),

$$\varepsilon_\alpha(t) = \kappa \delta(t) n_\alpha, \tag{21}$$

where κ is the strength of the applied field, n_α is a unit vector representing the orientation of the field, and $\delta(t)$ is the Dirac delta function. Although such a narrow impulse is non-physical, it modulates all frequencies (energies) equally and excites the system into all states simultaneously. An alternative approach is to use a harmonic function with a specific frequency,[18,21,23] which can also be enveloped with a Gaussian function.[14,22] Such harmonic perturbations may be used for studying a particular excitation (or a small set of excitations).

From a single real-time simulation with the electric field applied along a direction $\beta \in \{x, y, z\}$, three Cartesian components of the induced electric dipole moment are obtained using

$$\mu_{\alpha\beta}^{\text{ind}}(t) = \text{Tr} \left[\mathbf{P}_\alpha \mathbf{D}_\beta^{\text{MO}}(t) \right] - \mu_\alpha^{\text{static}}; \qquad \alpha \in \{x, y, z\}. \tag{22}$$

Here, $\mu_\alpha^{\text{static}} = \text{Tr} \left[\mathbf{P}_\alpha \mathbf{D}_0^{\text{MO}} \right]$ is the static dipole moment, and $\mathbf{D}_\beta^{\text{MO}}(t)$ is the time-evolved density matrix (see Section 2.2). In the most general case, we need to perform three distinct

simulations for each of the Cartesian direction β, although the total number of simulations can be reduced for symmetric molecules. The field-dependent dynamical dipole polarizability tensor $\boldsymbol{\alpha}(\omega)$ is then calculated from the Fourier transformed induced dipole moments $\boldsymbol{\mu}^{\text{ind}}(\omega)$ as

$$\alpha_{\alpha\beta}(\omega) = \frac{1}{\kappa}\mu_{\alpha\beta}^{\text{ind}}(\omega), \tag{23}$$

and the final absorption spectrum (the dipole strength function) $S(\omega)$ is obtained as

$$S(\omega) = \frac{4\pi\omega}{3c}\operatorname{Im}\operatorname{Tr}\left[\boldsymbol{\alpha}(\omega)\right]. \tag{24}$$

It is important to note that due to the non-perturbative formalism of RT-TDDFT, the dynamical dipole polarizability tensor depends on the external field and it can also contain higher-order responses (hyperpolarizabilities). In the present work, however, the results were evaluated for very small field strengths κ, for which the higher-order contamination disappears, and the dynamical polarizability reduces to the regular leading-order contribution. However, as shown by Ding et al.,[21] it is possible to extract frequency-dependent hyperpolarizabilities from the real-time simulations by using a finite-field method (a series of short simulations using monochromatic pulses).

In the limit of an infinite simulation time and infinitely small time steps, the Fourier transformation of the dipole moments results in a sum of Dirac delta-function peaks. Such simulations are, however, not achievable in practice. In order to partially rectify these limitations, and to ensure that all oscillations vanish before the simulation is stopped, we multiply the time-dependent dipole moment with a damping factor $e^{-\gamma t}$ before we transform it to the frequency domain. This introduces finite and identical lifetimes for all excited states, and the resulting spectra will display Lorentzian-shaped lines instead of delta-function-shaped lines. Note that this damping of the dipole moments is artificial and has no connection to the true lifetimes of the excited states. This would require the inclusion of different dissipation mechanisms in the Hamiltonian.

14

2.4 Analytic form for δ-function type perturbations

In order to evaluate the perturbation part of the Fock operator in Eq. (21), a numerical representation of the delta function must be chosen. One possibility is to use a rectangular representation. This will, however, lead to an improper description of higher frequencies in the final spectra due to the discontinuity at the edges of the rectangle. A smoother representation can be obtained by using a Gaussian function.[14,25]

In this work we use an alternative approach. We exploit the localized nature of the delta function, and split the task into two parts: First the ground-state density matrix is perturbed, and then it is propagated in time using only the unperturbed part of the Fock operator. The density matrix can be perturbed analytically, avoiding the need to find a numerical representation of $\delta(t)$. This contrasts with an approach in which the perturbation is considered as part of the time evolution, *i.e.* in which the ground-state density matrix is propagated using the perturbed Fock operator.

To justify the perturb-and-propagate scheme, we consider the following property of the evolution operator

$$\mathbf{U}(t'', t) = \mathbf{U}(t'', t') \, \mathbf{U}(t', t), \tag{25}$$

which follows from the definition of $\mathbf{U}(t, t')$ in Eq. (9). It allows us to study the propagation of the density matrix in an infinitely small time interval $\langle 0^-, 0^+ \rangle$.

To express the perturbed density matrix, let us split the Fock matrix

$$\mathbf{F}(t) = \mathbf{F}_0(t) + \tilde{\mathbf{P}}\delta(t), \tag{26}$$

where $\mathbf{F}_0(t)$ is the perturbation-independent part, and $\tilde{\mathbf{P}}$ is an arbitrary hermitian one-electron operator (in our case $\tilde{\mathbf{P}} = -\kappa\mathbf{P}$). The following relations hold for the evolution

operator and the perturbed density matrix [$\mathbf{D}_0^{\mathrm{MO}}$ is defined in Eq. (2)]

$$\mathbf{U}(0^+, 0^-) = e^{-i\tilde{\mathbf{P}}}, \tag{27}$$

$$\mathbf{D}(0^+) = e^{-i\tilde{\mathbf{P}}} \mathbf{D}_0^{\mathrm{MO}} e^{i\tilde{\mathbf{P}}}. \tag{28}$$

The proof of these relations, can be found in the Appendix.

2.5 Analysis of spectral transitions

In addition to the dipole moment, other time-dependent properties can be Fourier transformed to extract valuable electronic structure information from the real-time simulations. To reveal the nature of the electronic excitations in absorption spectra, we introduce in this section a dipole-weighted transition matrix analysis. The analysis is based on viewing the dipole strength function in Eq. (24) as a sum of ground-state molecular orbital pair contributions, which provides valuable insight into the intensity of individual spectral lines in terms of occupied–virtual MO pairs.

It is important to note that a Fourier component $T(\omega_0)$ of a time-domain signal $T(t)$ corresponding to a resonance frequency ω_0

$$T(\omega_0) = \int_{-\infty}^{\infty} T(t) e^{-i\omega_0 t} \mathrm{d}\, t, \tag{29}$$

contains information about a spectral line centered at this frequency. In our analysis, we use as the time-domain signal $T(t)$ the induced dipole moments in Eq. (22). Unlike Eq. (22), however, the induced dipole moments associated with the individual occupied(i)–virtual(a) pairs of molecular orbitals are not summated, but rather treated separately, such that

$$\mu_{ai}^{\mathrm{ind}}(t) = P_{ia} D_{ai}(t) + P_{ai} D_{ia}(t). \tag{30}$$

Here, we omit the Cartesian index for clarity. Using Eq. (29) to evaluate the Fourier com-

ponent of $\mu_{ai}^{\text{ind}}(t)$ at a specific resonance frequency, one can identify the contribution of individual occupied-virtual orbital pairs to the signal in the absorption spectra. In practice, one needs to select only a small set of occupied and virtual orbitals to reveal the nature of electronic excitations, as it will be illustrated in Section 4.

3   Computational details

The relativistic four-component RT-TDDFT method described in the previous section has been implemented in the ReSpect quantum chemistry program[48] and used for the calculation of absorption spectra of the group 12 atoms and the heavy-element hydrides (TlH, AuH). In the later case, the experimental ground-state equilibrium geometries ($r_{\text{Tl-H}} = 1.8702\,\text{Å}$, $r_{\text{Au-H}} = 1.52385\,\text{Å}$) were used.[49] All results have been obtained with the Dirac–Coulomb Hamiltonian and non-relativistic adiabatic DFT functionals of LDA type (SVWN(5)),[50,51] GGA type (BLYP),[52,53] and hybrid type (B3LYP).[53,54] The DFT contributions were evaluated numerically on an adaptive molecular grid (program default) and their rotational invariance was preserved by means of a non-collinear approach with the spin density described by the norm of the spin magnetization vector.[41] The molecular grid is a superposition of atomic grids, each consisting of 50 radial grid points and Lebedev's quadrature grid points of an adaptive size in the angular part, as formulated in Ref.[55]. In all calculations, we used for the large component the uncontracted all-electron VDZ basis sets of Dyall,[56–58] whereas the small-component basis was generated on-the-fly imposing the restricted kinetically balanced (RKB) relation.[35] For all nuclei, a finite-sized Gaussian model was used.[59] In order to reduce the cost of the dominant computational part, the evaluation of the two-electron contributions to the Fock matrix, we used an atom-pair approximation in the small-small block where the evaluation of four-center two-electron integrals over atom-centered small-component basis functions $\{\chi^S\}$ was discarded unless bra- and ket-basis pairs shared the same origin, i.e. $[\chi_A^S \chi_B^S | \chi_C^S \chi_D^S]\delta_{AB}\delta_{CD}$ where δ is the Kronecker delta and A, B, C, D refer

to the origin of basis functions. This approximation typically yields small errors in the total energy ($\lessgtr 10^{-5}E_h$) and speeds up the evaluation of the Fock matrix by a factor 2-3.

The theoretical modelling of optical absorption spectra by the RT-TDDFT approach as implemented in our program proceeds in two steps: initially, the SCF solutions of the time-independent Dirac–Kohn–Sham (DKS) equation are sought to obtain a ground-state one-electron density. In the second step, the real-time time-dependent DKS equation is solved using the second-order mid-point Magnus method with an analytic perturbation applied at time zero; see Sections 2.2 and 2.4 for more details. The convergence of the SCF step was controlled by the norm of the DIIS vector with a threshold of 10^{-8}, whereas the accuracy of the Magnus solver was controlled by an iterative extrapolation-interpolation scheme (Eqs. (18) and (19)) with the convergence criterion $|\mathbf{D}^{(n)}(t + \Delta t) - \mathbf{D}^{(n+1)}(t + \Delta t)| < 10^{-6}$. The use of this iterative extrapolation–interpolation scheme proved important in order to ensure the stability of the results obtained using the second-order mid-point Magnus propagator. Without this scheme, instabilities were observed, manifested either by a loss of energy conservation or by a large induced dipole moment even in the absence of external fields. The final absorption spectra were obtained from a Fourier transform of the induced dipole moments as described in Section 2.3, and the area under the spectral functions was normalized to unity (hence arbitrary units for intensities). All figures presented were plotted using Python's matplotlib library.[60]

4   Results and discussion

In this section, we apply our relativistic four-component implementation of RT-TDDFT to the calculation of vertical excitation energies of two closed-shell benchmark sets: the group 12 atoms (Zn, Cd, Hg) and the heavy-atom hydrides AuH and TlH. The goal is to validate the new methodology by comparing the RT-TDDFT results with experimental values and recent theoretical results obtained from relativistic two- and four-component

TDDFT calculations. Despite the fact the RT-TDDFT approach inherently contains non-linear effects, these features are not manifested in the results presented here due to weak electric field perturbations applied.

4.1 Excitation energies in Group 12 atoms (Zn, Cd, Hg)

The group 12 atoms Zn, Cd and Hg represent a series of closed-shell systems that have received much attention, experimentally as well as theoretically, due to the fine-structure splitting of the excited states. The most up-to-date collection of the atomic spectral lines observed experimentally has been tabulated by Sansonetti and Martin.[61] There have also been several theoretical studies of these atomic systems using LR-TDDFT, both at the four-component[30,31] and the two-component[62–66] relativistic level of theory.

The absorption spectra of the group 12 atoms were obtained from four-component RT-TDDFT simulations in which the electronic ground state with an ns^2 configuration was perturbed by an analytic δ-function pulse with strength $\kappa = 0.0005$ au (see Eq. (21)). The perturbed state was evolved for 30000 time steps of length 0.2 au, which corresponds to total simulation time of 145 fs and leads to an energy (frequency) resolution of ± 0.0285 eV in the calculated spectrum. During the time evolution, the induced dipole moments were evaluated on-the-fly and Fourier transformed from time to frequency domain at the end of the simulations to yield the final absorption spectrum, as illustrated in Figure 1.

The two lowest electronic excitations for the group 12 atoms correspond to the "spin-forbidden" $^1S_0 \rightarrow {}^3P_1$ and "spin-allowed" $^1S_0 \rightarrow {}^1P_1$ transitions and can be easily assigned based on the relative intensities. More interestingly, all theoretical works based on the linear-response TDDFT[30,31,62,63,65,66] also report states not present in our RT-TDDFT simulations, for instance, the triplet $^3P_2$ and $^3P_0$ states coming from the splitting of the virtual np orbitals due to spin–orbit coupling. In order to rationalize this difference, we note that in the LR-TDDFT calculations, the excited state energies are obtained as poles of the linear response functions. As such, all singly excited states can be determined by this method, in-

dependent of the transition probability. The transition probabilities can instead be obtained as residues of the linear response function. In contrasts, with a dipole perturbation only, the RT-TDDFT approach will only be able to access states with a non-vanishing dipole transition moment, and thus to some extent only address the states observable in a conventional absorption spectrum. Once transformed to the frequency domain, transitions to excited states with low or zero transition moments will not be observed in our calculations and we therefore observe fewer energy levels than in earlier LR-TDDFT works. The two lines in the RT-TDDFT absorption spectra agrees however very well with the experimentally observed persistent lines,[61] as well as with the selection rule that within the dipole approximation allows transitions between states with $\Delta J = 0, \pm 1$ except for the transition from $J = 0$ to $J = 0$, J being the total angular momentum of the electronic state.

In Table 1, we have collected the electronic excitation energies associated with the lowest $ns^2 \rightarrow ns^1 np^1$ transitions in the Zn, Cd, and Hg atoms together with available literature data. An interesting observation from Table 1 is that for the singlet-excited states, LDA provides in general results in very good agreement with experimental data. In contrast, LDA provides rather poor results for the triplet states, and exact exchange appears mandatory in order to provide good excitation energies for the triplet-excited state. Improvements are observed for BLYP compared to LDA for the triplet state, but the agreement with experiment is nevertheless significantly better for the B3LYP functional. We observe that our results in general are in excellent agreement with earlier theoretical results, and in particular with the results obtained by Bast *et al.*,[31] Wang *et al.*,[62] and Kühn *et al.*,[66] suggesting that the computational levels in these studies are equally sufficient for the considered molecules. We recall that the main differences between our data and those of earlier theoretical studies lies in the choice of the one-electron basis set. The good agreement with previous theoretical studies provides a confirmation of the correctness of our implementation and the quality of our computational results.

Figure 1: Time evolution of the dipole moment of mercury atom after the application of δ-type pulse (left) and the absorption spectrum with a notable singlet–triplet transition obtained after Fourier transform (right). Four-component real-time TDDFT (RT-TDDFT) computations.
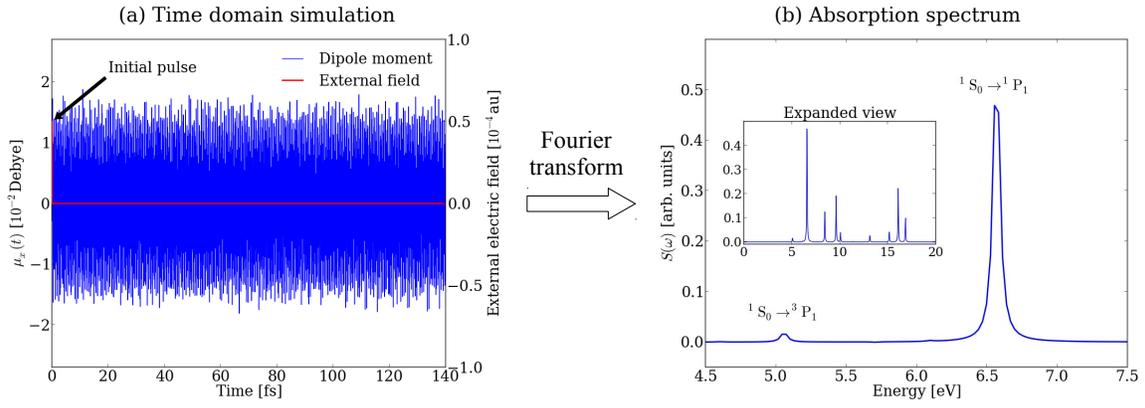

(a) Time domain simulation

(b) Absorption spectrum

Table 1: Calculated $ns^2 \rightarrow ns^1np^1$ excitation energies of group 12 atoms ($n = 4 - 6$ for Zn, Cd, Hg) (in eV). The present 4-component real-time TDDFT (RT-TDDFT) results are compared with the recent relativistic linear response TDDFT (LR-TDDFT) calculations and experimental data.

Atom	DFT	State	Excitation energy						
			RT-TDDFT	LR-TDDFT					Exp.[61]
			This work	Gao[a]	Bast[b]	Wang[c]	Nakata[d]	Kühn[e]	
Zn	LDA	$^1P_1$	5.84	6.07	5.76	5.76	6.20		5.80
	BLYP	$^1P_1$	5.78		5.61		6.14		
	B3LYP	$^1P_1$	5.73		5.58		6.03		
	LDA	$^3P_1$	4.30	4.40	4.35	4.35	4.41		4.03
	BLYP	$^3P_1$	4.27		4.25		4.32		
	B3LYP	$^3P_1$	4.05		4.04		4.14		
Cd	LDA	$^1P_1$	5.44	5.50	5.34	5.35	5.74	5.47	5.42
	BLYP	$^1P_1$	5.36		5.18		5.64		
	B3LYP	$^1P_1$	5.27		5.14		5.54		
	LDA	$^3P_1$	4.02	4.04	4.02	4.02	4.11	4.12	$(3.80)^f$
	BLYP	$^3P_1$	3.96		3.92		4.01		
	B3LYP	$^3P_1$	3.76		3.73		3.84		
Hg	LDA	$^1P_1$	6.56	6.66	6.53	6.53	6.85	6.57	6.70
	BLYP	$^1P_1$	6.41		6.30		6.69		
	B3LYP	$^1P_1$	6.35		6.27		6.62		
	LDA	$^3P_1$	5.06	5.12	5.08	5.09	5.26	5.12	4.89
	BLYP	$^3P_1$	4.96		4.94		5.13		
	B3LYP	$^3P_1$	4.73		4.73		4.94		

[a] all electron 4-component implementation based on Dirac–Coulomb Hamiltonian and Slater-type functions;[30]   [b] all electron 4-component implementation based on Dirac–Coulomb Hamiltonian and Gaussian-type functions;[31]   [c] all electron 2-component implementation based on ZORA Hamiltonian and Slater-type functions;[62]   [d] all electron 2-component implementation based on ZORA Hamiltonian and Gaussian-type functions;[65]   [e] 2-component implementation based on 2c-ECP and Gaussian-type functions;[66]   [f] non-persistent line according to Ref.[61]

4.2 Excitation energies in diatomic molecules (TlH, AuH)

Heavy-element hydrides are systems with a richer electronic structure than atoms, yet they are still sufficiently simple to be used as benchmark systems. We selected closed shell diatomic molecules TlH and AuH because the systems exhibit pronounced relativistic effects and have been previously used in the linear-response TDDFT benchmark calculations at the quasi-relativistic two-component level of theory by Wang et $al.$,[62] and at the fully relativistic four-component level of theory by Gao et $al.$[30] Moreover, high-quality experimental data are also available from Huber and Herzberg.[49] Note, no account is made of vibronic effects in our calculations and the evaluated absorption spectra contain only information about vertical excitation energies.

To obtain the absorption spectrum from four-component RT-TDDFT simulations, the electronic ground-state calculated in the absence of an external electric field was perturbed by an analytic δ-function pulse with strength 0.00001 au (see Eq. (21)). The perturbed state was evolved for 30000 time steps of length 0.15 au, which corresponds to total simulation time of 109 fs and leads to the energy (frequency) resolution of ± 0.0380 eV. During the time propagation, the induced dipole moments were evaluated on-the-fly and Fourier transformed from time to frequency domain at the end of the simulations to yield the final absorption spectrum, as illustrated in Figure 2 and Figure 3.

In the absence of spin–orbit coupling, the ground-state electronic configuration of TlH has the valence orbital occupation σ^2 where the HOMO σ orbital is composed of the p_z orbital of Tl and the s orbital of H. The LUMO is a π orbital composed of the p orbitals of thallium and hydrogen. Due to the spin-orbit coupling, the π orbitals are split into $\pi_{1/2}$ and $\pi_{3/2}$ levels. The calculated absorption spectrum of TlH is presented in Figure 2 and the corresponding data for the lowest vertical excitation energies are collected in Table 2. The first two lines can be assigned to the excitations from the doubly degenerate HOMO to the $\pi_{1/2}$ and $\pi_{3/2}$ virtual orbitals, respectively. This is confirmed by the dipole-weighted transition matrix analysis shown in Figure 2, where one can clearly see the most important occupied and

vacant orbitals involved in the transition, as well as by the 1:2 relative intensities of the lines, reflecting the degeneracies of the $\pi_{1/2}$ and $\pi_{3/2}$ orbitals. We note that the LR-TDDFT results of Wang *et al.*[62] include additional lines in this area not visible in our spectrum. This is due to the aforementioned difference between the RT and LR calculations: only allowed transitions can be obtained from the RT simulation. Experimentally, an additional line is observed at $3.02\,\text{eV}$, corresponding to the triplet-excited state. This line is too close to the singlet-excited state signal at $3.00\,\text{eV}$ to be distinguishable in our calculations due to the resolution limits, and besides it would be significantly weaker in intensity than the singlet line. Our results are in slightly better agreement with experiment than the results of Wang *et al.*[62] and the use of the hybrid functional further improves the agreement. Still the gap between lines **A** and **B** is slightly better in their work. In general these results support expectations of Wang *et al.*: "... as far as the excitations of the valence electrons are concerned, the error of the ZORA method in dealing with relativistic effects should be smaller than the error of the approximations inherent in the XC potential and XC kernel."[62]

The calculated absorption spectrum of AuH is presented in Figure 3 and the vertical excitations energies are compared with the results of other authors and available experimental data in Table 2. In the absence of spin–orbit coupling, the ground state of AuH around the equilibrium geometry is a closed-shell state of symmetry $^1\Sigma^+$ (in the Λ-S notation). Due to the spin-orbit interaction, the valence molecular orbitals of $^1\Sigma^+$ are split and the ground state $X0^+$ consists of the molecular bispinors:[30] $(1\sigma_{1/2})^2$ $(1\pi_{1/2})^2$ $(1\pi_{3/2})^2$ $(\delta_{3/2})^2$ $(\delta_{5/2})^2$ $(2\sigma_{1/2})^2$. The presence of several low-lying vacant molecular bispinors, in particular $3\sigma_{1/2}$, $2\pi_{1/2}$, $2\pi_{3/2}$, leads to a richer excitation pattern for AuH than TlH or group 12 atoms. The developed analysis in terms of dipole-weighted transitions confirms the observation for 3 out of 4 lowest separate lines in the absorption spectrum. Whereas the first spectral line, depicted as **A** in Figure 3, can be interpreted as transition from the doubly degenerate HOMO orbital $2\sigma_{1/2}$ (number 79 and 80) to the doubly degenerate LUMO orbital $3\sigma_{1/2}$ (number 81 and 82), other transitions have more complicated structure. For instance, the second excited

state 0^+ calculated with B3LYP at 4.48 eV is dominated by the $1\pi_{1/2} \rightarrow 3\sigma_{1/2}$ transition accompanying by excitations also from other valence molecular bispinors.

The use of hybrid DFT functional does not improve the agreement with experimental data. While in the case of TlH molecule LDA excitation energies are smaller than those obtained with the B3LYP functional, for AuH the situation is opposite. Since for both molecules the LDA results underestimate the experimental data the use of hybrid functional improves the results for TlH but worsen for AuH. The observed trends agree with results of other authors and available experimental data. The results of Wang *et al.*[62] and Gao *et al.*[30] are in slightly better agreement with experiment than our results. A few points can affect the comparison. One of them is related to the basis set quality, since both implementations involve Slater-type functions. The other point is the difference in the used approaches: RT-TDDFT versus LR-TDDFT. However we would prefer to postpone drawing any definitive conclusions before gaining more experience with different systems including those with charge transfer excitations.

Table 2: The vertical excitation energies of low-lying electronic states of TlH and AuH (in eV) . The present 4-component real-time TDDFT (RT-TDDFT) results are compared with the recent relativistic linear-response TDDFT (LR-TDDFT) calculations and experimental data. The excited states (in the ω–ω notation) are assigned to the spectral lines in Figure 2 and Figure 3 in square brackets.

Molecule	DFT	Excited state	Excitation energy				
			RT-TDDFT	LR-TDDFT			Exp.[49]
			This work	Wang[a]	Gao[b]	Kühn[c]	
TlH	LDA	[A] 0^+	2.07	2.08	—	2.09	2.20
	B3LYP		2.13				
	LDA	[B] 1	2.96	2.88	—	2.64	3.00
	B3LYP		3.04				
AuH	LDA	[A] 0^+	3.31	3.42	3.39	—	3.43
	B3LYP		3.19				
	LDA	[B] 0^+	4.52	4.70	4.66	—	4.78
	B3LYP		4.48				
	LDA	[C] 1	5.21	5.01	4.96	—	5.32
	B3LYP		5.05				

[a] all electron 2-component implementation based on ZORA Hamiltonian and Slater-type functions;[62] [b] all electron 4-component implementation based on Dirac–Coulomb Hamiltonian and Slater-type functions;[30] [c] 2-component implementation based on 2c-ECP and Gaussian-type functions;[66]

Figure 2: Top: Calculated absorption spectrum of TlH using the present 4-component real-time TDDFT (RT-TDDFT) approach. Bottom: Analysis of the fist two spectral lines in terms of ground state occupied–virtual MO contributions by means of a dipole-weighted transition matrix analysis (Section 2.5). The first line can be identified as HOMO to LUMO transition, whereas the second line as HOMO to LUMO+1 transition.
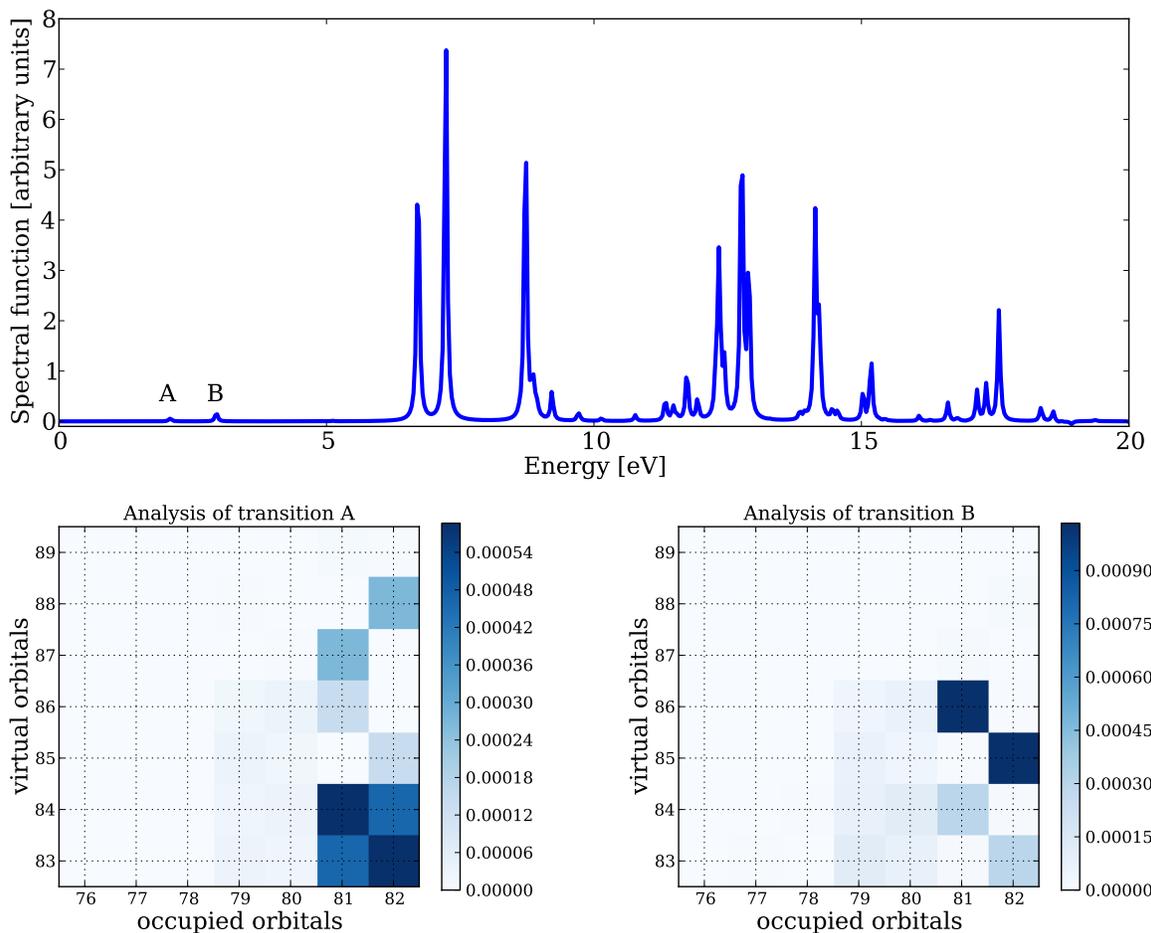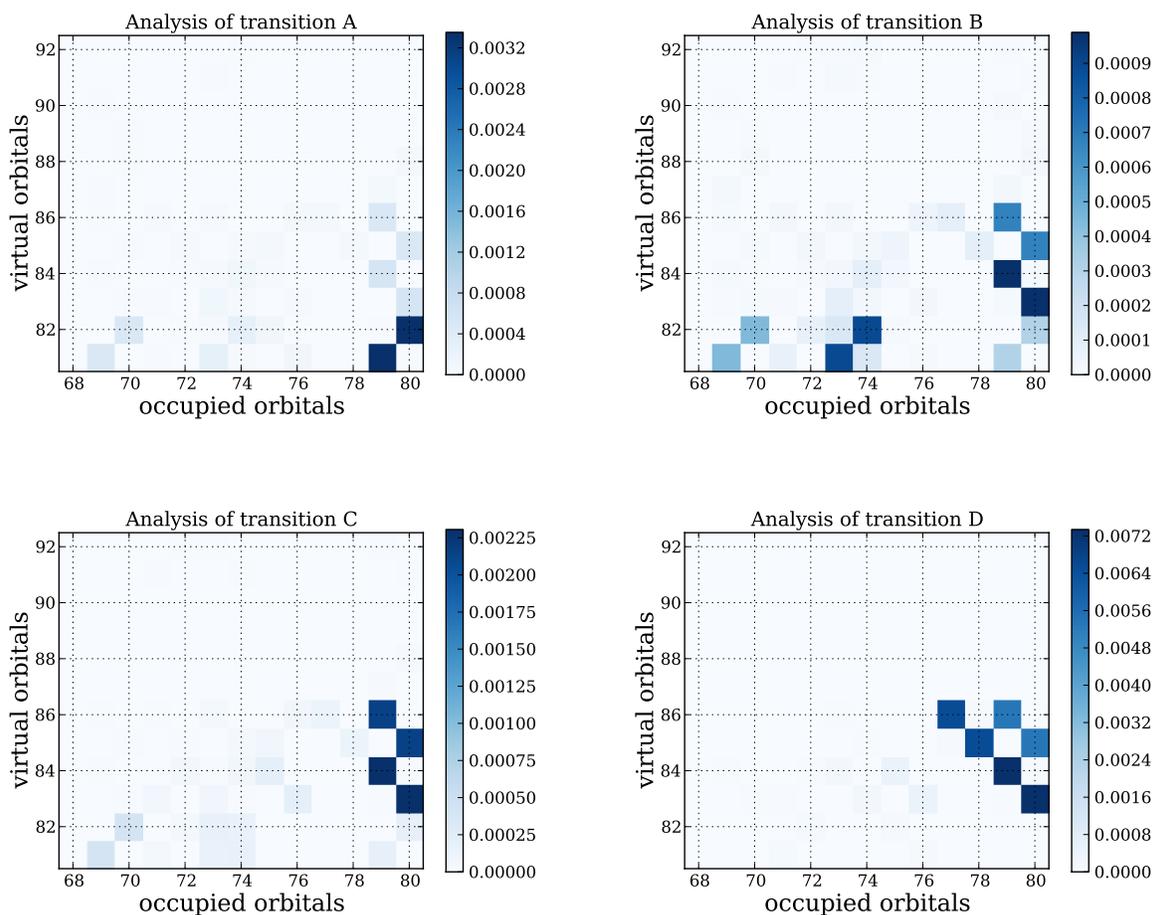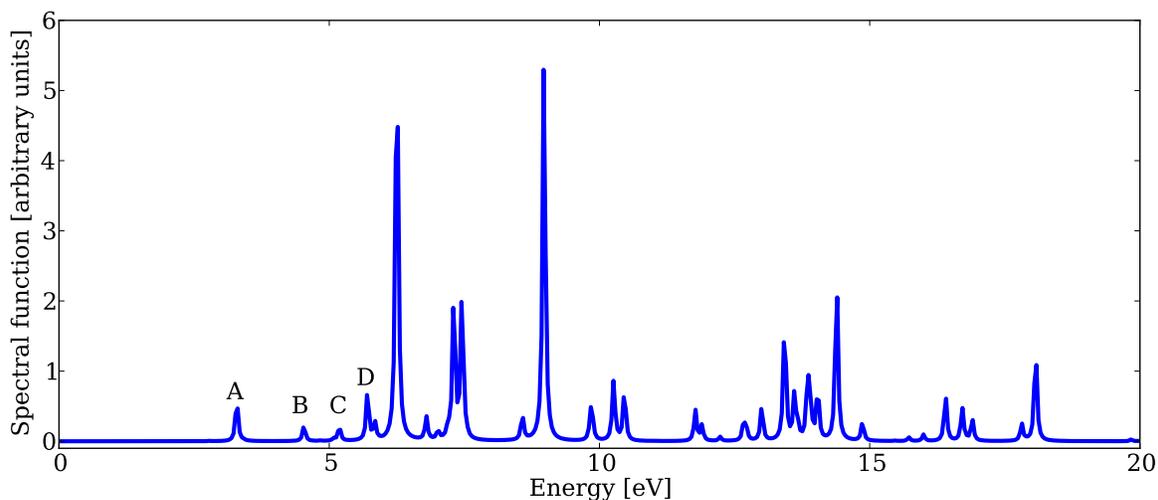
Figure 3: Top: Calculated absorption spectrum of AuH using the present 4-component real-time TDDFT (RT-TDDFT) approach. Bottom: Analysis of the fist four spectral lines in terms of ground state occupied–virtual MO contributions by means of a dipole-weighted transition matrix analysis (Section 2.5). The first line can be identified as HOMO to LUMO transition.

5 Summary and outlook

We have presented the first implementation of real-time time-dependent density functional theory at the relativistic four-component level of theory. The use of four-component relativistic theory in combination with RT-TDDFT has been made possible by matrix representation of the Dirac–Coulomb Hamiltonian using a time-independent basis of restricted kinetically balanced Gaussian-type functions, and fast techniques for evaluating two-electron integrals for restricted kinetically balanced basis sets.[36] To ensure numerical stability of the implementation, a second-order Magnus expansion in combination with an analytic representation of the delta-shaped pulse describing the applied external electric field has been implemented and used. We have also proposed a dipole-weighted transition matrix analysis facilitating the interpretation of spectral transitions in terms of ground-state molecular orbitals.

The applicability of this new implementation has been demonstrated by calculations of the valence electronic absorption spectrum of the group 12 atoms (Zn, Cd and Hg) as well as on two heavy-element hydrides (AuH and TlH). These systems have served as important benchmarks for the calculation of electronic absorption spectra using relativistic methods due to their fairly simple electronic spectrum, the importance of relativistic effects in these systems and the availability of experimental data of high quality.

We have demonstrated that our calculations reproduce well earlier relativistic four-component studies for which linear response theory has been used to calculate the excitation energies. This is in agreement with expectations, as RT-TDDFT and LR-TDDFT should give the same absorption spectra in the frequency domain if the computational methodology is the same. Test calculations also showed that in the weak-field limit the dipole-weighted transition matrix analysis of RT-TDDFT gives the same character of vertical excitations as the LR-TDDFT approach. It is furthermore interesting to note that the LDA gives the best agreement with experiment for the lowest singlet-excited state of the group 12 atoms, whereas exact exchange through the use of a hybrid functional is mandatory in order to get reasonable agreement with experiment for the lowest triplet-excited state. For TlH and AuH

molecules the situation is more complicated: the hybrid functional improves results for TlH but worsen for AuH.

Whereas both LR-TDDFT and RT-TDDFT provides in the frequency domain identical results, RT-TDDFT gives access to all excited states with the same computational complexity, independently of whether we are considering valence-excited states or core-excited states. In the later case special computational techniques must be often used, such as the complex polarization propagator technique[67] or Lanczos algorithms for selected energy regions.[68]

RT-TDDFT also allows fast electronic processes to be studied. With recent experimental advances, it is now possible to follow electronic rearrangements with attosecond resolution,[69] and RT-TDDFT can be a useful technique for providing additional insight into the changes occurring in the electronic density at this time scale. Combining the propagation of the electron density with nuclear dynamics in *ab initio* Ehrenfest dynamics[70–72] will also provide a unique opportunity to explore fast chemical processes. In combination with a relativistic description of the electron density, for which spin-orbit effects are included variationally, this can provide a unique tool for studying spectroscopic techniques such as femtosecond stimulated Raman spectroscopy[73] or complex chemical processes such as light-induced spin-crossover processes.[74]

Finally, the inclusion of relativistic effects variationally, and in particular spin–orbit effects, will allow us to explore important spectral regions observed in X-ray spectroscopy. In particular the L_2 and L_3 edges of near-edge X-ray absorption spectroscopy requires a variational treatment of spin–orbit effects in order to reproduce the splitting of the $2p$ orbitals into $2p_{1/2}$ and $2p_{3/2}$ orbitals. A first theoretical study of the X-ray absorption spectrum of SF_6 obtained with the RT-TDDFT approach have recently been performed by our group.[75]

6   Appendix: Proof of the analytic form for δ-function type perturbations

In order to prove the statement made in Section 2.4

$$\mathbf{U}(0^+, 0^-) = e^{-i\tilde{\mathbf{P}}}, \tag{31}$$

let us consider the time-dependent equation for the evolution operator[42]

$$i\frac{\partial}{\partial t}\mathbf{U}(t, t') = \mathbf{F}(t)\mathbf{U}(t, t'), \tag{32}$$

where t and t' are arbitrary times, and $\mathbf{U}(t', t') = \mathbf{1}$ is the initial condition. Alternatively, the integral form of Eq. (32) can be written as

$$\mathbf{U}(t, t') = \mathbf{1} - i\int_{t'}^{t} \mathbf{F}(\tau)\mathbf{U}(\tau, t')d\tau. \tag{33}$$

We solve this equation iteratively

$$\mathbf{U}^{(k+1)}(t, t') = \mathbf{1} - i\int_{t'}^{t} \mathbf{F}^{(k)}(\tau)\mathbf{U}^{(k)}(\tau, t')d\tau, \tag{34}$$

where

$$\mathbf{F}^{(k)}(\tau) = \mathbf{F}_0^{(k)}(\tau) + \tilde{\mathbf{P}}\delta(\tau), \tag{35}$$

$$\mathbf{F}_0^{(k)}(\tau) \equiv \mathbf{F}_0\left(\mathbf{D}^{(k)}(\tau)\right), \tag{36}$$

$$\mathbf{D}^{(k)}(\tau) = \mathbf{U}^{(k)}(\tau, t')\mathbf{D}_0^{\text{MO}}\mathbf{U}^{(k)\dagger}(\tau, t'), \tag{37}$$

$$\mathbf{U}^{(0)}(\tau, t') = \mathbf{1}. \tag{38}$$

Let $t' = -\Delta$ where $0 < \Delta \ll 1$. Our aim is to evaluate the limit

$$\lim_{\Delta \to 0^+} \lim_{k \to \infty} \mathbf{U}^{(k)}(\Delta, -\Delta) \equiv \mathbf{U}(0^+, 0^-). \tag{39}$$

To first order we obtain

$$\mathbf{U}^{(1)}(\Delta, -\Delta) = \mathbf{1} - i\tilde{\mathbf{P}} - i \int_{-\Delta}^{\Delta} \mathbf{F}_0^{(0)}(\tau) d\tau = \mathbf{1} - i\tilde{\mathbf{P}} + O(\Delta), \tag{40}$$

where $\mathbf{F}_0^{(0)}$ is the ground-state Fock matrix. Similarly, using Eq. (34), we can write the second order contribution as

$$\mathbf{U}^{(2)}(\Delta, -\Delta) = \mathbf{1} - i \int_{-\Delta}^{\Delta} \mathbf{F}_0^{(1)}(\tau) d\tau - i\tilde{\mathbf{P}} +$$

$$+ (-i)^2 \int_{-\Delta}^{\Delta} d\tau_1 \int_{-\Delta}^{\tau_1} d\tau_2 \mathbf{F}_0^{(1)}(\tau_1) \mathbf{F}_0^{(0)}(\tau_2) +$$

$$+ (-i)^2 \int_{0}^{\Delta} \mathbf{F}_0^{(1)}(\tau) d\tau \tilde{\mathbf{P}} +$$

$$+ (-i)^2 \tilde{\mathbf{P}} \int_{-\Delta}^{0} \mathbf{F}_0^{(0)}(\tau) d\tau +$$

$$+ (-i\tilde{\mathbf{P}})^2 \int_{-\Delta}^{\Delta} d\tau_1 \int_{-\Delta}^{\tau_1} d\tau_2 \delta(\tau_1) \delta(\tau_2). \tag{41}$$

Since $\mathbf{D}^{(1)}(\tau)$ and $\mathbf{F}_0^{(1)}(\tau)$ are bounded functions of time, albeit discontinuous at $\tau = 0$, all integrals over $\mathbf{F}_0^{(0)}$ and $\mathbf{F}_0^{(1)}$ can be shown to be proportional to Δ, and thus vanish in the limit of $\Delta \to 0^+$. The final term can be evaluated using

$$\int_{-\Delta}^{\Delta} d\tau_1 \int_{-\Delta}^{\tau_1} d\tau_2 \delta(\tau_1) \delta(\tau_2) = \frac{1}{2} \int_{-\Delta}^{\Delta} d\tau_1 \int_{-\Delta}^{\Delta} d\tau_2 \delta(\tau_1) \delta(\tau_2) = \frac{1}{2} \tag{42}$$

which leads to

$$\mathbf{U}^{(2)}(\Delta, -\Delta) = \mathbf{1} - i\tilde{\mathbf{P}} + \frac{1}{2}(-i\tilde{\mathbf{P}})^2 + O(\Delta). \tag{43}$$

To express $\mathbf{U}^{(k)}$ we need to generalize Eq. (42) to

$$\int_{-\Delta}^{\Delta} d\tau_1 \int_{-\Delta}^{\tau_1} d\tau_2 \ldots \int_{-\Delta}^{\tau_{k-1}} d\tau_k \delta(\tau_1) \ldots \delta(\tau_k) = \frac{1}{k!}, \tag{44}$$

which is implied by the fact that the integrand is the same for each integration region defined by a permutation of $(\tau_1, \ldots, \tau_2)$. Finally, we obtain

$$\mathbf{U}^{(k)}(\Delta, -\Delta) = \sum_{j=0}^{k} \frac{(-i\tilde{\mathbf{P}})^j}{j!} + O_k(\Delta) \tag{45}$$

where O_k is, in principle, a different function of Δ for each k approaching zero if $\Delta \to 0^+$. If we assume convergence of the iterative scheme, and hence the existence of the limit $k \to \infty$ in Eq. (39), we recover the result in Eq. (31).

Acknowledgement

References

(1) Helgaker, T.; Coriani, S.; Jørgensen, P.; Kristensen, K.; Olsen, J.; Ruud, K. *Chem. Rev.* **2012**, *112*, 543–631.

(2) Runge, E.; Gross, E. K. U. *Phys. Rev. Lett.* **1984**, *52*, 997.

(3) Gross, E. K. U.; Kohn, W. *Phys. Rev. Lett.* **1985**, *55*, 2850.

(4) Casida, M. E. In *Recent Advances in Density Functional Methods, Part I*; Chong, D. P., Ed.; World Scientific: Singapure, 1995; pp 155–192.

(5) Dreuw, A.; Head-Gordon, M. *Chem. Rev.* **2005**, *105*, 4009–4037.

(6) XVIIIth International Conference on Ultrafast Phenomena. 2013.

(7) Theilhaber, J. *Phys. Rev.* **B 1992**, *46*, 12990.

(8) Yabana, K.; Bertsch, G. *Phys. Rev.* **B 1996**, *54*, 4484.

(9) Castro, A.; Appel, H.; Oliveira, M.; Rozzi, C. A.; Andrade, X.; Lorenzen, F.; Marques, M. A.; Gross, E.; Rubio, A. *Phys. Status Solidi B* **2006**, *243*, 2465–2488.

(10) Soler, J. M.; Artacho, E.; Gale, J. D.; García, A.; Junquera, J.; Ordejón, P.; Sánchez-Portal, D. *J. Phys.: Condens. Matter* **2002**, *14*, 2745.

(11) Sun, J.; Song, J.; Zhao, Y.; Liang, W.-Z. *J. Chem. Phys.* **2007**, *127*, 234107.

(12) Meng, S.; Kaxiras, E. *J. Chem. Phys.* **2008**, *129*, 054110.

(13) Akama, T.; Imamura, Y.; Nakai, H. *Chem. Lett.* **2010**, *39*, 407–409.

(14) Lopata, K.; Govind, N. *J. Chem. Theory Comput.* **2011**, *7*, 1344–1355.

(15) Tsolakidis, A.; Sánchez-Portal, D.; Martin, R. *Phys. Rev.* **B 2002**, *66*, 235416.

(16) Baer, R.; Neuhauser, D. *J. Chem. Phys.* **2004**, *121*, 9803–9807.

(17) Yabana, K.; Nakatsukasa, T.; Iwata, J.-I.; Bertsch, G. F. *Phys. Status Solidi B* **2006**, *243*, 1121–1138.

(18) Wang, F.; Yam, C. Y.; Chen, G. *J. Chem. Phys.* **2007**, *126*, 244102.

(19) Takimoto, Y.; Vila, F. D.; Rehr, J. J. *J. Chem. Phys.* **2007**, *127*, 154114.

(20) Liu, J.; Guo, Z.; Sun, J.; Liang, W. *Front. Chem. China* **2010**, *5*, 11–28.

(21) Ding, F.; Van Kuiken, B. E.; Eichinger, B. E.; Li, X. *J. Chem. Phys.* **2013**, *138*, 064104.

(22) Cheng, C.-L.; Evans, J. S.; Van Voorhis, T. *Phys. Rev.* **B 2006**, *74*, 155112.

(23) Isborn, C. M.; Li, X. *J. Chem. Theory Comput.* **2009**, *5*, 2415–2419.

(24) Lee, K.-M.; Yabana, K.; Bertsch, G. *J. Chem. Phys.* **2011**, *134*, 144106.

(25) Lopata, K.; Van Kuiken, B. E.; Khalil, M.; Govind, N. *J. Chem. Theory Comput.* **2012**, *8*, 3284–3292.

(26) Nobusada, K.; Yabana, K. *Phys. Rev.* **A 2007**, *75*, 032518.

(27) Gao, B.; Ruud, K.; Luo, Y. *J. Chem. Phys.* **2012**, *137*, 194307.

(28) Ekström, U.; Visscher, L.; Bast, R.; Thorvaldsen, A. J.; Ruud, K. *J. Chem. Theory Comput.* **2010**, *6*, 1971–1980.

(29) Gao, J.; Liu, W.; Song, B.; Liu, C. *J. Chem. Phys.* **2004**, *121*, 6658–6666.

(30) Gao, J.; Zou, W.; Liu, W.; Xiao, Y.; Peng, D.; Song, B.; Liu, C. *J. Chem. Phys.* **2005**, *123*, 054102.

(31) Bast, R.; Jørgen, H.; Jensen, A. A.; Saue, T. *Int. J. Quantum Chem.* **2009**, *109*, 2091–2112.

(32) Selstø, S.; Lindroth, E.; Bengtsson, J. *Phys. Rev.* **A 2009**, *79*, 043418.

(33) Belpassi, L.; Storchi, L.; Quiney, H. M.; Tarantelli, F. *Phys. Chem. Chem. Phys.* **2011**, *13*, 12368–12394.

(34) McWeeny, R. *Methods of molecular quantum mechanics*, 2nd ed.; Academic Press: London, 1992; pp 438–442.

(35) Stanton, R. E.; Havriliak, S. *J. Chem. Phys.* **1984**, *81*, 1910–1918.

(36) Repisky, M. *InteRest 2.0, An integral program for relativistic quantum chemistry* **2013**,

(37) Komorovsky, S.; Repisky, M.; Malkina, O. L.; Malkin, V. G.; Malkin Ondík, I.; Kaupp, M. *J. Chem. Phys.* **2008**, *128*, 104101.

(38) Ishikawa, Y.; Quiney, H. M.; Malli, G. L. *Phys. Rev.* **A 1991**, *43*, 3270–3278.

(39) Saue, T.; Faegri, K.; Helgaker, T.; Gropen, O. *Mol. Phys.* **1997**, *91*, 937–950.

(40) Saue, T.; Helgaker, T. *J. Comput. Chem.* **2002**, *23*, 814–823.

(41) van Wüllen, C. *J. Comput. Chem.* **2002**, *23*, 779–785.

(42) Tannor, D. J. *Introduction to Quantum Mechanics: A Time-Dependent Perspective*; University Science Books: Sausalito, 2007; pp 185–196.

(43) Kosloff, R. *J. Phys. Chem.* **1988**, *92*, 2087–2100.

(44) Castro, A.; Marques, M. a. L.; Rubio, A. *J. Chem. Phys.* **2004**, *121*, 3425–33.

(45) Lubich, C. *From quantum to classical molecular dynamics: reduced models and numerical analysis*; European Mathematical Society: Zürich, 2008; pp 63–104.

(46) Magnus, W. *Comm. Pure Appl. Math.* **1954**, *7*, 649–673.

(47) Bernadotte, S.; Atkins, A. J.; Jacob, C. R. *J. Chem. Phys.* **2012**, *137*, 204106.

(48) **ReSpect**, version 3.4.0, 2014 – Relativistic Spectroscopy DFT program of authors Repisky M.; Komorovsky S.; Malkin V. G.; Malkina O. L.; Kaupp M.; Ruud K., with contributions from Bast R.; Ekstrom U.; Kadek M.; Knecht S.; Konecny L.; Malkin Ondik I.; Malkin E. See http://rel-qchem.sav.sk, (accessed Jan 8, 2015).

(49) Huber, K.-P.; Herzberg, G. *Constants of diatomic molecules*; Springer US, 1979; pp 8–689.

(50) Slater, J. C. *Phys. Rev.* **1951**, *81*, 385.

(51) Vosko, S. H.; Wilk, L.; Nusair, M. *Can. J. Phys.* **1980**, *58*, 1200–1211.

(52) Becke, A. D. *Phys. Rev.* **A 1988**, *38*, 3098.

(53) Lee, C.; Yang, W.; Parr, R. G. *Phys. Rev.* **B 1988**, *37*, 785.

(54) Becke, A. D. *J. Chem. Phys.* **1993**, *98*, 5648–5652.

(55) Krack, M.; Köster, A. M. *J. Chem. Phys.* **1998**, *108*, 3226–3234.

(56) Dyall, K. G.; Gomes, A. S. P. unpublished.

(57) Dyall, K. G. *Theor. Chem. Acc.* **2007**, *117*, 483–489.

(58) Dyall, K. G.; Gomes, A. S. P. *Theor. Chem. Acc.* **2010**, *125*, 97–100.

(59) Visscher, L.; Dyall, K. G. *At. Data Nucl. Data Tables* **1997**, *67*, 207–224.

(60) Hunter, J. D. *Computing In Science & Engineering* **2007**, *9*, 90–95.

(61) Sansonetti, J. E.; Martin, W. C. *J. Phys. Chem. Ref. Data* **2005**, *34*, 1559–2259.

(62) Wang, F.; Ziegler, T.; van Lenthe, E.; van Gisbergen, S.; Baerends, E. J. *J. Chem. Phys.* **2005**, *122*, 204103.

(63) Peng, D.; Zou, W.; Liu, W. *J. Chem. Phys.* **2005**, *123*, 144101.

(64) Devarajan, A.; Gaenko, A.; Autschbach, J. *J. Chem. Phys.* **2009**, *130*, 194102.

(65) Nakata, A.; Tsuneda, T.; Hirao, K. *J. Chem. Phys.* **2011**, *135*, 224106.

(66) Kuhn, M.; Weigend, F. *J. Chem. Theory Comput.* **2013**, *9*, 5341–5348.

(67) Ekström, U.; Norman, P.; Carravetta, V.; Ågren, H. *Phys. Rev. Lett.* **2006**, *97*, 143001.

(68) Coriani, S.; Fransson, T.; Christiansen, O.; Norman, P. *J. Chem. Theory Comput.* **2012**, *8*, 1616–1628.

(69) Neidel, C.; Klei, J.; Yang, C.-H.; Rouzée, A.; Vrakking, M. J. J.; Klünder, K.; Miranda, M.; Arnold, C. L.; Fordell, T.; L'Huillier, A.; Gisselbrecht, M.; Johnsson, P.; Dinh, M. P.; Suraud, E.; Reinhard, P.-G.; Despré, V.; Marques, M. A. L.; Lépine, F. *Phys. Rev. Lett.* **2013**, *111*, 033001.

(70) Li, X.; Tully, J. C.; Schlegel, H. B.; Frisch, M. J. *J. Chem. Phys.* **2005**, *123*, 084106.

(71) Jakowski, J.; Morokuma, K. *J. Chem. Phys.* **2009**, *130*, 224106.

(72) Andrade, X.; Castro, A.; Zueco, D.; Alonso, J. L.; Echenique, P. *J. Chem. Theory Comput.* **2009**, *5*, 728–742.

(73) Kukura, P.; McCamant, D. W.; Yoon, S.; Wandschneider, D. B.; Mathies, R. A. *Science* **2005**, *310*, 1006–1009.

(74) Decurtins, S.; Gütlich, P.; Hasselbach, K. M.; Hauser, A.; Spiering, H. *Inorg. Chem.* **1985**, *24*, 2174–2178.

(75) Kadek, M.; Repisky, M.; Konecny, L.; Gao, B.; Ruud, K. *in preparation*

Figure 4: For Table of Contents Only